Simulation of Sound Absorption by Scattering Bodies Treated with Acoustic Liners Using a Time-Domain Boundary Element Method

Michelle E. Pizzo* and Fang Q. Hu†
Department of Mathematics and Statistics, Old Dominion University, Norfolk, VA 23529, USA

Douglas M. Nark‡
Structural Acoustics Branch, NASA Langley Research Center, Hampton, VA 23681, USA

Reducing aircraft noise is a major objective in the field of computational aeroacoustics. When designing next generation quiet aircraft, it is important to be able to accurately and efficiently predict the acoustic scattering by an aircraft body from a given noise source. Acoustic liners are an effective tool for aircraft noise reduction, and are characterized by a complex-valued frequency-dependent impedance, $Z(\omega)$. Converted into the time-domain using Fourier transforms, an impedance boundary condition can be used to simulate the acoustic wave scattering of geometric bodies treated with acoustic liners. This work uses an admittance boundary condition where the admittance, $Y(\omega)$, is defined to be the inverse of impedance, i.e., $Y(\omega) = 1/Z(\omega)$. An admittance boundary condition will be derived and coupled with a time-domain boundary integral equation. The solution will be obtained iteratively using spatial and temporal basis functions and will allow for acoustic scattering problems to be modeled with geometries consisting of both un-lined and soft surfaces. Stability will be demonstrated through eigenvalue analysis.

Nomenclature

$p(\boldsymbol{r}_s, \omega)$	=	Acoustic Pressure in the Frequency-Domain
$p(\boldsymbol{r}, t)$	=	Acoustic Pressure in the Time-Domain
$v(\boldsymbol{r}_s, \omega)$	=	Acoustic Velocity in the Frequency-Domain
$u(\boldsymbol{r}, t)$	=	Acoustic Velocity in the Time-Domain
$\boldsymbol{r}'$	=	Arbitrary Point on Scattering Body Surface
ρ_0	=	Average Fluid Density
BEM	=	Boundary Element Method
BIE	=	Boundary Integral Equation
$-\cot\left(\frac{1}{2}\omega\nu\Delta t - i\frac{1}{2}\epsilon\right)$	=	Cavity Reactance
$\partial/\partial\tilde{n}$	=	Combined Normal Derivative
$\tilde{a}, \tilde{b}$	=	Constants Used to Determine the Stability Condition
ϵ	=	Damping in the Cavity's Fluid
N_x, N_y, and N_z	=	Discretization of the Scattering Body in the x-, y-, and z-directions
E_j	=	Element on Scattering Body
λ	=	Eigenvalue
ωm	=	Face-Sheet Mass Reactance
F_R	=	Face-Sheet Resistance
$\tilde{G}(\boldsymbol{r}, t; \boldsymbol{r}', t')$	=	Free Space Adjoint Green's Function
i	=	Imaginary Unit, ($i^2 = -1$)
$\boldsymbol{n}$	=	Inward Normal Vector on the Scattering Body

*Ph.D. Candidate and NASA Langley Research Center High Performance Computing Incubator Member, michelle.e.pizzo@nasa.gov
†Professor and AIAA Associate Fellow
‡Senior Research Scientist and AIAA Associate Fellow

$q(\boldsymbol{r}, t)$	=	Known Acoustic Source
$\boldsymbol{M}$	=	Mach Number
$\boldsymbol{B}, \boldsymbol{C}, \boldsymbol{D}, \boldsymbol{E}$	=	Matrix Notation for the Uncoupled System of Equations
$\boldsymbol{A}$	=	Matrix Notation for the Coupled System of Equations
$\boldsymbol{U}$	=	Mean Flow
$\partial/\partial\overline{n}$	=	Modified Normal Derivative
$\nu\Delta t = 2L/c$	=	Multiple of the Time-Step and Proportional to Two Times the Cavity Depth, L
V_s	=	Region of Acoustic Surfaces
t'_R	=	Retarded Time
S_0	=	Rigid Scattering Surface
F_β	=	Parameter Used for Varying the Cavity Reactance
$\boldsymbol{r}'_s$	=	Point on the Scattering Surface Boundary
S	=	Scattering Surface
$\boldsymbol{u^n}, \boldsymbol{v^n}, \boldsymbol{w^n}$	=	Solutions for the Discretized System of Equations
c	=	Speed of Sound
$\phi_j(\boldsymbol{r}_s)$	=	Surface Element Basis Functions at Node j
$Y(\omega)$, $y(t)$	=	Surface Admittance, in the Frequency- and Time- Domain
$Z(\omega)$, $z(t)$	=	Surface Impedance
$\psi_k(t)$	=	Temporal Basis Functions at Time k
$r = (x, y, z)$	=	Three-Dimensional Point in Space
TD-BEM	=	Time-Domain Boundary Element Method
TD-BIE	=	Time-Domain Boundary Integral Equation
t	=	Time
Δt	=	Time-Step
N_e	=	Total Number of Surface Nodes
N_t	=	Total Number of Time Steps
V	=	Volume Exterior of the Scattering Surface

I. Introduction

Reducing aircraft noise is a major objective in the field of computational aeroacoustics. When designing next generation quiet aircraft, it is important to be able to accurately and efficiently predict the acoustic scattering by an aircraft body from a given noise source [1–4]. Acoustic scattering problems can be modeled using boundary element methods (BEMs) by reformulating the linear convective wave equation as a boundary integral equation (BIE), both in the frequency-domain and the time-domain; BEMs reduce the spatial dimension by one by allowing for the integration over a surface instead of a volume [5–10].

Frequency-domain solvers are the most commonly used and researched within literature; they have a reduced computational cost [11] and allow for modeling time-harmonic fields at a single frequency [10–12]. Moreover, frequency-domain solvers eliminate the growth of Kelvin-Helmholtz instabilities caused by velocity shear of two interacting fluids, and allow for an impedance boundary condition to be imposed more naturally [12].

Despite the benefits of frequency-domain solvers, there are several distinct advantages to using a time-domain solver [1, 13]. Time-domain solvers allow for the simulation and study of broadband sources and time-dependent transient signals, whereas studying broadband sources in the frequency-domain, on the other hand, carry a high computational cost. Time-domain solvers also allow for the scattering solutions at all frequencies to be obtained within a single computation and avoid needing to invert a large dense linear system as is required in the frequency-domain. Moreover, a time-domain solution is more naturally coupled with a nonlinear computational fluid dynamics simulation of noise sources.

Time-domain BIEs (TD-BIEs) have an intrinsic numerical instability due to resonant frequencies resulting from non-trivial solutions in the interior domain and carry a high computational cost. In recent years, numerical techniques for modeling acoustic wave scattering by complex geometries using a TD-BIE have been under development [1–4]. It has been shown that stability can be realized under a Burton-Miller type reformulation of the TD-BIE. Moreover, the computational cost can be reduced using fast algorithms and high performance computing. In this work, a time-domain BEM (TD-BEM) will be used to solve a TD-BIE reformulated from the convective wave equation; the scattering solution will be obtained using temporal and surface basis functions and a March-On-in-Time scheme in which a sparse matrix is

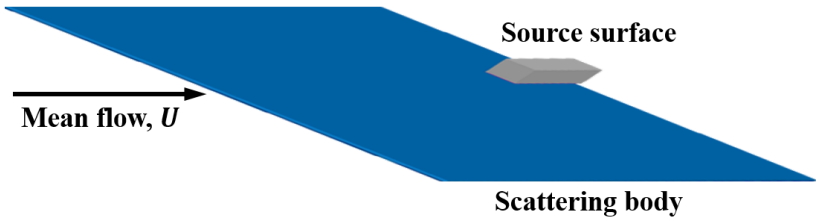

Fig. 1 Schematic diagram illustrating the relationship between the mean flow, the surface of the scattering body, and the surface of the acoustic source.

solved iteratively.

In this work, acoustic scattering problems are considered for geometric bodies consisting of both rigid and soft surfaces. Soft surfaces are treated with acoustic liners; these liners are incredibly effective at absorbing sound in a specified frequency band [13–15]. Acoustic liners are typically composed of an array of Helmholtz resonators, used for dissipating the incident acoustic wave [13–15], and are characterized by a frequency-dependent impedance value, herein denoted by $Z(\omega)$. Impedance is a complex-valued quantity; $\mathrm{Re}(Z)$ is given to be the acoustic resistance and $\mathrm{Im}(Z)$ is given to be the acoustic reactance [13–15].

Given that impedance is a frequency-dependent quantity, it must be transformed into the time-domain for time-domain analysis [13]. In [14], a frequency-domain impedance boundary condition is transformed to the time-domain using Fourier transforms. This work is motivated by [14], and proposes to instead use an admittance boundary condition transformed to the time-domain using Fourier transforms. Admittance, $Y(\omega)$, is defined as the the inverse of impedance:

$$Y(\omega) = \frac{1}{Z(\omega)}.$$

A time-domain representation of admittance, $y(t)$, will be derived and coupled with the TD-BIE March-On-in-Time scheme using temporal and spatial basis functions. The solution will allow for acoustic scattering problems to be modeled with both rigid (un-lined) and soft (lined) surfaces.

In Section II, a TD-BIE is derived with suitable boundary conditions for scattering bodies with both rigid and soft surfaces. In Section III, we derive a stable Burton-Miller type reformulation of the TD-BIE and discuss the stability of the resulting TD-BEM for rigid body problems. An admittance boundary condition used for soft surfaces is derived in Section IV and the coupling of this system to the stable Burton-Miller TD-BEM is discussed in Section V. In Section VI stability is demonstrated for the coupled system. Concluding remarks and future work are discussed in Section VII.

II. Derivation of the Time Domain Boundary Integral Equation

In the present study, we aim to accurately and efficiently predict the scattering of a sound field by an object from a given noise source in the presence of a constant mean flow as shown in Figure 1. Acoustic waves are assumed to be disturbances of small amplitudes. With a constant mean flow, the acoustic disturbances are governed by the convective wave Eq. [16], written as follows:

$$\left(\frac{\partial}{\partial t} + \boldsymbol{U}\cdot\nabla\right)^2 p - c^2\nabla^2 p = q\left(\boldsymbol{r}, t\right) \tag{1}$$

with homogeneous initial conditions:

$$p(\boldsymbol{r}, 0) = \frac{\partial p}{\partial t}(\boldsymbol{r}, 0) = 0, \;\; t = 0 \tag{2}$$

where $p(\boldsymbol{r}, t)$ is the acoustic pressure, $q(\boldsymbol{r}, t)$ is the known acoustic source, and c is the speed of sound. Equations (1) and (2) are to be supplemented with boundary conditions on the scattering surface. These conditions will be discussed further in this section.

It is well known that the convective wave equation (1) and the initial conditions (2), along with suitable boundary conditions, can be reformulated into an integral equation. By introducing a free-space adjoint Green's function $\tilde{G}(\boldsymbol{r}, t; \boldsymbol{r'}, t')$ that, for convenience of discussion, is defined as follows:

$$\left(\frac{\partial}{\partial t} + \boldsymbol{U}\cdot\nabla\right)^2 \tilde{G} - c^2\nabla^2\tilde{G} = \delta\left(\boldsymbol{r} - \boldsymbol{r'}, t - t'\right) \tag{3}$$

with homogeneous initial conditions:

$$\tilde{G}(\boldsymbol{r}, t; \boldsymbol{r'}, t') = \frac{\partial \tilde{G}}{\partial t}(\boldsymbol{r}, t; \boldsymbol{r'}, t') = 0, \ t > t', \tag{4}$$

the wave propagation problem can be reformulated into a TD-BIE. Note that $\tilde{G}(\boldsymbol{r}, t; \boldsymbol{r'}, t')$ is nonzero for $t \in (-\infty, t']$. The solution to Eqs. (3) and (4) is well-known and, for a mean flow of a general direction, can be written as [17]:

$$\tilde{G}(\boldsymbol{r}, t; \boldsymbol{r'}, t') = \frac{G_0}{4\pi c^2} \, \delta \left(t' - t + \boldsymbol{\beta} \cdot (\boldsymbol{r'} - \boldsymbol{r}) - \frac{\overline{R}}{c\alpha^2} \right) \tag{5}$$

where

$$\overline{R}(\boldsymbol{r}, \boldsymbol{r'}) = \sqrt{\left| \boldsymbol{M} \cdot (\boldsymbol{r} - \boldsymbol{r'}) \right|^2 + \alpha^2 \left| \boldsymbol{r} - \boldsymbol{r'} \right|^2}, \ G_0 = \frac{1}{\overline{R}(\boldsymbol{r}, \boldsymbol{r'})} \tag{6}$$

in which

$$\boldsymbol{M} = \frac{\boldsymbol{U}}{c}, \ \alpha = \sqrt{1 - M^2}, \ \boldsymbol{\beta} = \frac{\boldsymbol{M}}{1 - M^2} \tag{7}$$

In Eqs. (5) through (7), $M = |\boldsymbol{M}|$ is the magnitude of Mach number $\boldsymbol{M}$, $U = |\boldsymbol{U}|$ is the magnitude of mean flow $\boldsymbol{U}$, and $\boldsymbol{r'}$ is an arbitrary point on scattering body surface.

To reformulate the wave propagation problem into a TD-BIE, we perform an operation of $\tilde{G} \times (1) - p \times (3)$, integrate over the volume V exterior of the scattering surface S for space, integrate over an interval $[0^-, t'^+]$ for time t, and apply the Divergence Theorem. We then get an expression for the acoustic pressure p at an arbitrary point r' in V and time t' as follows:

$$p(\boldsymbol{r'}, t') = \int_{0^-}^{t'^+} \int_V \tilde{G} q(\boldsymbol{r}, t) \, d\boldsymbol{r} \, dt + c^2 \int_{0^-}^{t'^+} \int_S \left(\tilde{G} \frac{\partial p}{\partial \overline{n}} - p \frac{\partial \tilde{G}}{\partial \overline{n}} \right) d\boldsymbol{r}_s \, dt - c \int_{0^-}^{t'^+} \int_S \left(\tilde{G} \frac{\partial p}{\partial t} - p \frac{\partial \tilde{G}}{\partial t} \right) M_n \, d\boldsymbol{r}_s \, dt \tag{8}$$

where $\partial / \partial \overline{n} = \partial / \partial n - M_n (\boldsymbol{M} \cdot \nabla) = (\boldsymbol{n} - M_n \boldsymbol{M}) \cdot \nabla$ denotes a *modified normal derivative*, $\overline{\boldsymbol{n}} = \boldsymbol{n} - M_n \boldsymbol{M}$, and $M_n = \boldsymbol{M} \cdot \boldsymbol{n} = \boldsymbol{n} \cdot \boldsymbol{U} / c$ such that $\boldsymbol{n}$ is the inward normal vector on the scattering body S. Equation (8) is the Kirchhoff integral representation of the acoustic field in the presence of a uniform mean flow.

As shown in [17], with the introduction of a *combined normal derivative*, $\partial / \partial \tilde{n} = \partial / \partial \overline{n} - (M_n / c) \, \partial / \partial t$, noting that:

$$\frac{\partial \tilde{G}}{\partial \tilde{n}} = \frac{1}{4\pi c^2} \frac{\partial G_0}{\partial \overline{n}} \left[\delta \left(t' - t + \boldsymbol{\beta} \cdot (\boldsymbol{r'} - \boldsymbol{r}) - \frac{\overline{R}}{c\alpha^2} \right) + \frac{\overline{R}}{c\alpha^2} \delta' \left(t' - t + \boldsymbol{\beta} \cdot (\boldsymbol{r'} - \boldsymbol{r}) - \frac{\overline{R}}{c\alpha^2} \right) \right],$$

the integral relation in Eq. (8) can be further expressed as an integration of retarded time values ${t_R}'$ by utilizing $\tilde{G}$ as given in Eq. (5):

$$p(\boldsymbol{r'}, t') = \frac{1}{4\pi c^2} \int_{V_s} \frac{1}{\overline{R}} q(\boldsymbol{r}, t'_R) \, d\boldsymbol{r} + \frac{1}{4\pi} \int_S \left[G_0 \frac{\partial p}{\partial \tilde{n}}(\boldsymbol{r}_s, t'_R) - \frac{\partial G_0}{\partial \overline{n}} \left(p(\boldsymbol{r}_s, t'_R) + \frac{\overline{R}}{c\alpha^2} \frac{\partial p}{\partial t}(\boldsymbol{r}_s, t'_R) \right) \right] d\boldsymbol{r}_s \tag{9}$$

where V_s denotes the region of acoustic surfaces and the retarded time is defined as $t'_R = t' + \boldsymbol{\beta} \cdot (\boldsymbol{r'} - \boldsymbol{r}) - \overline{R} / (c\alpha^2)$. Equation (9) relates the solution at point $\boldsymbol{r'}$ and time t' to the direct contribution from source function q and a surface contribution involving the retarded time values of p and their normal derivatives. When both $p(\boldsymbol{r}_s, t)$ and $\partial p / \partial \tilde{n}(\boldsymbol{r}_s, t)$ on surface S are known, $p(\boldsymbol{r'}, t')$ at any field point $\boldsymbol{r'}$ can be computed using Eq. (9).

However, $p(\boldsymbol{r}_s, t)$ and $\partial p / \partial \tilde{n}(\boldsymbol{r}_s, t)$ are not independent. They have to satisfy the BIE formed when $\boldsymbol{r'}$ is taken to be a boundary point $\boldsymbol{r}'_s$. The TD-BIE therefore results by taking the limit of Eq. (9) as $\boldsymbol{r'} \to \boldsymbol{r}'_s$ where $\boldsymbol{r}'_s$ is a point on the boundary and $\boldsymbol{r}_s$ is some arbitrary point. Assuming that $\boldsymbol{r}'_s$ is a smooth boundary collocation point, the resulting TD-BIE is given by [17]:

$$\frac{1}{c^2} \int_{V_s} \frac{1}{\overline{R}} q(\boldsymbol{r}, t'_R) \, d\boldsymbol{r} = 2\pi p(\boldsymbol{r}'_s, t') - \int_S \left[G_0 \frac{\partial p}{\partial \tilde{n}}(\boldsymbol{r}_s, t'_R) - \frac{\partial G_0}{\partial \overline{n}} \left(p(\boldsymbol{r}_s, t'_R) + \frac{\overline{R}}{c\alpha^2} \frac{\partial p}{\partial t}(\boldsymbol{r}_s, t'_R) \right) \right] d\boldsymbol{r}_s. \tag{10}$$

The left-hand-side of Eq. (10) denotes the contribution from the external sources to the surface point $\boldsymbol{r}'_s$. The integral on the right-hand-side denotes the contribution from the source surface and scattering surface.

For sound scattering problems, $p(\boldsymbol{r}'_s, t')$ on the scattering surface S is determined by Eq. (10) when the boundary condition for p on S is given. Unlike the work presented in [17] where the boundary condition for p is that of rigid surfaces, in this work, we assume that the scattering surface S consists of both rigid surfaces — denoted herein by S_0 — and soft surfaces — denoted herein by S_l, i.e., $S = S_0 \cup S_l$. On rigid surfaces, we impose the Zero Energy Flux [17] boundary condition:

$$\frac{\partial p}{\partial \tilde{n}}(\boldsymbol{r}_s, t) = 0, \ \boldsymbol{r}_s \in S_0. \tag{11}$$

On soft surfaces, $\partial p/\partial \tilde{n}$ is a non-zero term herein denoted by P_n, i.e.,

$$\frac{\partial p}{\partial \tilde{n}}(\boldsymbol{r}_s, t) = \left\{ \begin{array}{ll} P_n(\boldsymbol{r}_s, t), & \boldsymbol{r}_s \in S_l \\ 0, & \boldsymbol{r}_s \in S_0 \end{array} \right\} \tag{12}$$

For simplicity, we assume $M_n = 0$ on soft surfaces; i.e., we assume that the mean flow is always tangent to the surface wherever the liner is installed. Under this assumption, $\partial p/\partial \tilde{n}$ is equal to $\partial p/\partial n$.

III. Derivation of the Stable Burton-Miller Type Boundary Element Method

The TD-BIE for solid wall boundary conditions has been known to have an intrinsic numerical instability due to resonant frequencies resulting from non-trivial solutions in the interior domain. Using a Burton-Miller type reformulation of Eq. (10), resonant frequencies can be eliminated and stability achieved [1–4]. The Burton-Miller type reformulation will now be applied to the TD-BIE with liner boundary condition. The reformulation results from taking the derivative of Eq. (10) in the form of:

$$\tilde{a}\frac{\partial}{\partial t} + \tilde{b}c\frac{\partial}{\partial \tilde{n}'}$$

where $\tilde{a}$ and $\tilde{b}$ define the stability condition, $\tilde{a}/\tilde{b} < 0$ [17].

Specifically, applying the above operator to Eq. (9) and taking the limit $\boldsymbol{r}' \to \boldsymbol{r}'_s$, we get:

$$\begin{aligned}
&\tilde{a}\left[2\pi\frac{\partial p}{\partial t}(\boldsymbol{r}'_s, t') - \int_{S_l} G_0(\boldsymbol{r}_s, \boldsymbol{r}')\frac{\partial P_n}{\partial t}(\boldsymbol{r}_s, t'_R)d\boldsymbol{r}_s + \int_S \frac{\partial G_0}{\partial \bar{n}}(\boldsymbol{r}_s, \boldsymbol{r}')\left(\frac{\partial p}{\partial t}(\boldsymbol{r}_s, t'_R) + \frac{\bar{R}}{c\alpha^2}\frac{\partial p}{\partial t^2}(\boldsymbol{r}_s, t'_R)\right)d\boldsymbol{r}_s\right] \\
&+\tilde{b}c\left[4\pi\frac{\partial p}{\partial \tilde{n}'}(\boldsymbol{r}'_s, t') - \frac{\partial}{\partial \tilde{n}'}\int_{S_l} G_0(\boldsymbol{r}_s, \boldsymbol{r}')P_n(\boldsymbol{r}_s, t'_R)d\boldsymbol{r}_s + \frac{\partial}{\partial \tilde{n}'}\int_S \frac{\partial G_0}{\partial \bar{n}}(\boldsymbol{r}_s, \boldsymbol{r}')\left(p(\boldsymbol{r}_s, t'_R) + \frac{\bar{R}}{c\alpha^2}\frac{\partial p}{\partial t}(\boldsymbol{r}_s, t'_R)\right)d\boldsymbol{r}_s\right]_{\boldsymbol{r}'=\boldsymbol{r}'_s} \\
&\qquad = \tilde{a}\frac{\partial Q}{\partial t'}(\boldsymbol{r}'_s, t') + \tilde{b}c\frac{\partial Q}{\partial \tilde{n}'}(\boldsymbol{r}'_s, t')
\end{aligned} \tag{13}$$

where $Q(\boldsymbol{r}'_s, t')$ denotes the source term appearing on the left hand side of (10). Note that we have:

$$\frac{\partial P_n}{\partial \tilde{n}'}(\boldsymbol{r}_s, t'_R) = \frac{\partial P_n}{\partial t}(\boldsymbol{r}_s, t'_R)\frac{\partial t'_R}{\partial \tilde{n}'} = \frac{\partial P_n}{\partial t}(\boldsymbol{r}_s, t'_R)\frac{\partial t'_R}{\partial \tilde{n}'}$$

which yields

$$\frac{\partial}{\partial \tilde{n}'}\int_{S_l} G_0(\boldsymbol{r}_s, \boldsymbol{r}')P_n(\boldsymbol{r}_s, t'_R)d\boldsymbol{r}_s = \int_{S_l}\frac{\partial G_0}{\partial \bar{n}'}(\boldsymbol{r}_s, \boldsymbol{r}')P_n(\boldsymbol{r}_s, t'_R)d\boldsymbol{r}_s + \int_{S_l} G_0(\boldsymbol{r}_s, \boldsymbol{r}')\frac{\partial P_n}{\partial t}(\boldsymbol{r}_s, t'_R)\frac{\partial t'_R}{\partial \tilde{n}'}d\boldsymbol{r}_s$$

where

$$\begin{aligned}
\frac{\partial t'_R}{\partial \tilde{n}'} &= \left(\frac{\partial}{\partial n'} - \frac{M_{n'}}{c}\left(\frac{\partial}{\partial t'} + \boldsymbol{U}\cdot\nabla\right)\right)\left(t' + \boldsymbol{\beta}\cdot(\boldsymbol{r}' - \boldsymbol{r}_s) - \frac{\bar{R}}{c\alpha^2}\right) \\
&= -\frac{M_{n'}}{c} + \boldsymbol{\beta}\cdot(\boldsymbol{n}' - M_{n'}\boldsymbol{M}) - \frac{1}{c\alpha^2}\frac{\partial \bar{R}}{\partial \bar{n}} = -\frac{M_{n'}}{c} + \frac{\boldsymbol{M}}{c\alpha^2}\cdot(\boldsymbol{n}' - M_{n'}\boldsymbol{M}) - \frac{1}{c\alpha^2}\frac{\partial \bar{R}}{\partial \bar{n}'} \\
&= -\frac{M_{n'}}{c} + \frac{1}{c\alpha^2}(M_{n'} - M_{n'}M^2) - \frac{1}{c\alpha^2}\frac{\partial \bar{R}}{\partial \bar{n}} = -\frac{M_{n'}}{c} + \frac{M_{n'}}{c\alpha^2}(1 - M^2) - \frac{1}{c\alpha^2}\frac{\partial \bar{R}}{\partial \bar{n}} = -\frac{1}{c\alpha^2}\frac{\partial \bar{R}}{\partial \bar{n}'}
\end{aligned}$$

and

$$\frac{\partial \bar{R}}{\partial \bar{n}'} = -\bar{R}^2\frac{\partial G_0}{\partial \bar{n}'}$$

$$G_0 \frac{\partial \bar{R}}{\partial \bar{n}'} = -\bar{R} \frac{\partial G_0}{\partial \bar{n}'}.$$

Then, Eq. (13) becomes:

$$\begin{aligned}
&\tilde{a}\left[2\pi \frac{\partial p}{\partial t}(\boldsymbol{r}'_s, t') - \int_{S_l} G_0(\boldsymbol{r}_s, \boldsymbol{r}') \frac{\partial P_n}{\partial t}(\boldsymbol{r}_s, t'_R) d\boldsymbol{r}_s + \int_S \frac{\partial G_0}{\partial \bar{n}}(\boldsymbol{r}_s, \boldsymbol{r}') \left(\frac{\partial p}{\partial t}(\boldsymbol{r}_s, t'_R) + \frac{\bar{R}}{c\alpha^2} \frac{\partial p}{\partial t^2}(\boldsymbol{r}_s, t'_R)\right) d\boldsymbol{r}_s\right] \\
&+\tilde{b}c\left[4\pi \frac{\partial p}{\partial \bar{n}'}(\boldsymbol{r}'_s, t') - \int_{S_l} \frac{\partial G_0}{\partial \bar{n}'}(\boldsymbol{r}_s, \boldsymbol{r}') P_n(\boldsymbol{r}_s, t'_R) d\boldsymbol{r}_s - \int_{S_l} G_0(\boldsymbol{r}_s, \boldsymbol{r}') \frac{\partial P_n}{\partial t}(\boldsymbol{r}_s, t'_R) \left(-\frac{1}{c\alpha^2} \frac{\partial \bar{R}}{\partial \bar{n}'}\right) d\boldsymbol{r}_s\right]_{\boldsymbol{r}' \to \boldsymbol{r}'_s} \\
&-\frac{\tilde{b}}{c\alpha^4} \int_S \bar{R}^3 \frac{\partial G_0}{\partial \bar{n}'} \frac{\partial G_0}{\partial \bar{n}} \frac{\partial^2 p}{\partial t^2}(\boldsymbol{r}_s, t'_R) d\boldsymbol{r}_s + \tilde{b}c\left[\int_S \frac{\partial^2 G_0}{\partial \bar{n}' \partial \bar{n}} \left(p(\boldsymbol{r}_s, t'_R) - p(\boldsymbol{r}'_s, t') + \frac{\bar{R}}{c\alpha^2} \frac{\partial p}{\partial t}(\boldsymbol{r}_s, t'_R)\right) d\boldsymbol{r}_s\right]_{\boldsymbol{r}' \to \boldsymbol{r}'_s} \\
&\qquad = \tilde{a} \frac{\partial Q}{\partial t'}(\boldsymbol{r}'_s, t') + \tilde{b}c \frac{\partial Q}{\partial \bar{n}'}(\boldsymbol{r}'_s, t').
\end{aligned} \tag{14}$$

The integrals involving p have been simplified in the same way as shown in [17]. The limit of the weakly singular integral involving P_n in the above can be found as follows. Let:

$$\begin{aligned}
&\lim_{\boldsymbol{r}' \to \boldsymbol{r}'_s} \int_S \frac{\partial G_0}{\partial \bar{n}'}(\boldsymbol{r}_s, \boldsymbol{r}') P_n(\boldsymbol{r}_s, t'_R) d\boldsymbol{r}_s \\
&= \lim_{\boldsymbol{r}' \to \boldsymbol{r}'_s} \int_S \left[\frac{\partial G_0}{\partial \bar{n}'}(\boldsymbol{r}_s, \boldsymbol{r}') + \frac{\partial G_0}{\partial \bar{n}}(\boldsymbol{r}_s, \boldsymbol{r}')\right] P_n(\boldsymbol{r}_s, t'_R) d\boldsymbol{r}_s - \lim_{\boldsymbol{r}' \to \boldsymbol{r}'_s} \int_S \frac{\partial G_0}{\partial \bar{n}}(\boldsymbol{r}_s, \boldsymbol{r}') P_n(\boldsymbol{r}_s, t'_R) d\boldsymbol{r}_s.
\end{aligned} \tag{15}$$

Note that

$$\frac{\partial G_0}{\partial \bar{n}'}(\boldsymbol{r}_s, \boldsymbol{r}') + \frac{\partial G_0}{\partial \bar{n}}(\boldsymbol{r}_s, \boldsymbol{r}') = \bar{\boldsymbol{n}}' \cdot \nabla' G_0 + \bar{\boldsymbol{n}} \cdot \nabla G_0 = -(\bar{\boldsymbol{n}}' - \bar{\boldsymbol{n}}) \cdot \nabla G_0$$

where we have used the fact that $\nabla' G_0 = -\nabla G_0$. With a weakened singularity, the first integral in (15) is continuous, giving:

$$\lim_{\boldsymbol{r}' \to \boldsymbol{r}'_s} \int_S \left[\frac{\partial G_0}{\partial \bar{n}'}(\boldsymbol{r}_s, \boldsymbol{r}') + \frac{\partial G_0}{\partial \bar{n}}(\boldsymbol{r}_s, \boldsymbol{r}')\right] P_n(\boldsymbol{r}_s, t'_R) d\boldsymbol{r}_s = \int_S \left[\frac{\partial G_0}{\partial \bar{n}'}(\boldsymbol{r}_s, \boldsymbol{r}'_s) + \frac{\partial G_0}{\partial \bar{n}}(\boldsymbol{r}_s, \boldsymbol{r}'_s)\right] P_n(\boldsymbol{r}_s, t'_R) d\boldsymbol{r}_s.$$

For the second integral in (15), it is known to be discontinuous and we have:

$$\lim_{\boldsymbol{r}' \to \boldsymbol{r}'_s} \int_S \frac{\partial G_0}{\partial \bar{n}}(\boldsymbol{r}_s, \boldsymbol{r}') P_n(\boldsymbol{r}_s, t'_R) d\boldsymbol{r}_s = \int_S \frac{\partial G_0}{\partial \bar{n}}(\boldsymbol{r}_s, \boldsymbol{r}'_s) P_n(\boldsymbol{r}_s, t'_R) d\boldsymbol{r}_s - 2\pi P_n(\boldsymbol{r}'_s, t'),$$

the details of which are given in [17]. Hence, we get:

$$\lim_{\boldsymbol{r}' \to \boldsymbol{r}'_s} \int_S \frac{\partial G_0}{\partial \bar{n}'}(\boldsymbol{r}_s, \boldsymbol{r}') P_n(\boldsymbol{r}_s, t'_R) d\boldsymbol{r}_s = \int_S \frac{\partial G_0}{\partial \bar{n}'}(\boldsymbol{r}_s, \boldsymbol{r}'_s) P_n(\boldsymbol{r}_s, t'_R) d\boldsymbol{r}_s + 2\pi P_n(\boldsymbol{r}'_s, t').$$

Then, by applying the above limit, we have the following Burton-Miller type reformulation of the TD-BIE:

$$\begin{aligned}
&\tilde{a}\left[2\pi \frac{\partial p}{\partial t}(\boldsymbol{r}'_s, t') - \int_{S_l} G_0(\boldsymbol{r}_s, \boldsymbol{r}') \frac{\partial P_n}{\partial t}(\boldsymbol{r}_s, t'_R) d\boldsymbol{r}_s + \int_S \frac{\partial G_0}{\partial \bar{n}}(\boldsymbol{r}_s, \boldsymbol{r}') \left(\frac{\partial p}{\partial t}(\boldsymbol{r}_s, t'_R) + \frac{\bar{R}}{c\alpha^2} \frac{\partial p}{\partial t^2}(\boldsymbol{r}_s, t'_R)\right) d\boldsymbol{r}_s\right] \\
&\qquad +\tilde{b}c\left[2\pi P_n(\boldsymbol{r}'_s, t') - \int_{S_l} \frac{\partial G_0}{\partial \bar{n}'}(\boldsymbol{r}_s, \boldsymbol{r}'_s) \left(P_n(\boldsymbol{r}_s, t'_R) + \frac{\bar{R}}{c\alpha^2} \frac{\partial P_n}{\partial t}(\boldsymbol{r}_s, t'_R)\right) d\boldsymbol{r}_s\right] \\
&-\frac{\tilde{b}}{c\alpha^4} \int_S \bar{R}^3 \frac{\partial G_0}{\partial \bar{n}'} \frac{\partial G_0}{\partial \bar{n}} \frac{\partial^2 p}{\partial t^2}(\boldsymbol{r}_s, t'_R) d\boldsymbol{r}_s + \tilde{b}c\left[\int_S \frac{\partial^2 G_0}{\partial \bar{n}' \partial \bar{n}} \left(p(\boldsymbol{r}_s, t'_R) - p(\boldsymbol{r}'_s, t') + \frac{\bar{R}}{c\alpha^2} \frac{\partial p}{\partial t}(\boldsymbol{r}_s, t'_R)\right) d\boldsymbol{r}_s\right] \\
&\qquad = \tilde{a} \frac{\partial Q}{\partial t'}(\boldsymbol{r}'_s, t') + \tilde{b}c \frac{\partial Q}{\partial \bar{n}'}(\boldsymbol{r}'_s, t').
\end{aligned} \tag{16}$$

In the above derivation, it is assumed that P_n is automatically zero at any rigid surface points.

The stable Burton-Miller type reformulation (16) is discretized by dividing S into boundary elements using surface element basis functions $\phi_j(\boldsymbol{r}_s)$ at node j and temporal basis functions $\psi_k(t)$ at time k:

$$p(\boldsymbol{r}_s, t) = \sum_{k=0}^{N_t} \sum_{j=1}^{N_e} u_j^k \phi_j(\boldsymbol{r}_s)\psi_k(t), \text{ and} \tag{17}$$

$$P_n(\boldsymbol{r}_s, t) = \sum_{k=0}^{N_t} \sum_{j=1}^{N_e} v_j^k \phi_j(\boldsymbol{r}_s)\psi_k(t) \tag{18}$$

where $v_j^k \equiv 0$ by default on any element E_j on rigid surfaces S_0. In Eqs. (17) and (18), N_e denotes the total number of surface nodes and N_t denotes the number of time-steps.

Let the spatial and temporal basis functions be defined as follows:

$$\phi_j(\boldsymbol{r}_s) = \left\{ \begin{array}{ll} 1, & \boldsymbol{r}_s \text{ on element } E_j \text{ that contains node } \boldsymbol{r_j} \\ 0, & \text{otherwise} \end{array} \right\} \tag{19}$$

$$\psi_k(t) = \Psi\left(\frac{t - t_k}{\Delta t}\right),\ \Psi(\tau) = \left\{ \begin{array}{ll} 1 + \frac{11}{6}\tau + \tau^2 + \frac{1}{6}\tau^3, & -1 < \tau \leq 0 \\ 1 + \frac{1}{2}\tau - \tau^2 - \frac{1}{2}\tau^3, & 0 < \tau \leq 1 \\ 1 - \frac{1}{2}\tau - \tau^2 + \frac{1}{2}\tau^3, & 1 < \tau \leq 2 \\ 1 - \frac{11}{6}\tau + \tau^2 - \frac{1}{6}\tau^3, & 2 < \tau \leq 3 \\ 0, & \text{otherwise} \end{array} \right\} \tag{20}$$

By evaluating the discretized Burton-Miller type reformulation at collocation points $\boldsymbol{r}_s = \boldsymbol{r}_i$ and time-step $t' = t_n$, we obtain the following system of equations:

$$\boldsymbol{B_0 u^n + C_0 v^n = q^n - B_1 u^{n-1} - C_1 v^{n-1} - B_2 u^{n-2} - C_2 v^{n-2} - \ldots - B_J u^{n-J} - C_J v^{n-J}} \tag{21}$$

where $\boldsymbol{u}^k$ and $\boldsymbol{v}^k$ denote the vector that contains all unknowns $\left\{u_j^k,\ j = 1, ..., N_e\right\}$ and $\left\{v_j^k,\ j = 1, ..., N_e\right\}$, respectively, at time level t_k. The non-zero entries for $\boldsymbol{B}$ and $\boldsymbol{C}$ are, respectively:

$$\begin{aligned} \{\boldsymbol{B_k}\}_{ij} = {} & 2\pi\tilde{a}\delta_{ij}\psi'_{n-k}(t_n) + \tilde{a}\int_{E_j} \frac{\partial G_0}{\partial \overline{n}} \left(\psi'_{n-k}(t_R^n) + \frac{\overline{R}}{c\alpha^2}\psi''_{n-k}(t_R^n)\right) d\boldsymbol{r}_s - \tilde{b}c\delta_{ij}\delta_{k0}\int_{S-E_i} \frac{\partial^2 G_0}{\partial \overline{n}'\partial \overline{n}}(\boldsymbol{r}_s, \boldsymbol{r}_i)\, d\boldsymbol{r_s} \\ & + \tilde{b}c\int_{E_j} \frac{\partial^2 G_0}{\partial \overline{n}'\partial \overline{n}} \left(\psi_{n-k}(t_R^n) - \delta_{ij}\psi_{n-k}(t_n) + \frac{\overline{R}}{c\alpha^2}\psi'_{n-k}(t_R^n)\right) d\boldsymbol{r}_s \\ & + \frac{\tilde{b}}{c\alpha^4}\int_{E_j} \overline{R}^3 \frac{\partial G_0}{\partial \overline{n}'}\frac{\partial G_0}{\partial \overline{n}}\psi''_{n-k}(t_R^n)\, d\boldsymbol{r}_s \text{ and} \end{aligned}$$

$$\{\boldsymbol{C_k}\}_{ij} = -\tilde{a}\int_{E_j} G_0(\boldsymbol{r}_s, \boldsymbol{r}'_s)\psi'_{n-k}(t'_R)\, d\boldsymbol{r}_s + 2\pi\tilde{b}c\delta_{ij}\psi_{n-k}(t_n) - \tilde{b}c\int_{E_j} \frac{\partial G_0}{\partial \overline{n}'} \left(\psi_{n-k}(t_R^n) + \frac{\overline{R}}{c\alpha^2}\psi'_{n-k}(t_R^n)\right) d\boldsymbol{r}_s,$$

where δ_{ij} and δ_{k0} are Kronecker delta functions and a prime in the above denotes a derivative with respect to time. Equation (21) is a system of equations with two unknowns. In order to obtain solutions for u^k and v^k, a second system of equations is required. The second system results from the discretization of the liner admittance boundary condition.

Recall that $v_j^k \equiv 0$ by default on any element E_j on rigid surfaces S_0. Assuming rigid body scattering only, a solution to Eq. (21) can be obtained for u^k. In [17], it was demonstrated through eigenvalue analysis that stability is achieved for rigid bodies when using the Burton-Miller type reformulation of the TD-BIE, and that direct solution of the equation without Burton-Miller type reformulation can lead to unstable solutions. In the present work, we aim to demonstrate through eigenvalue analysis that, for scattering bodies with both rigid and soft surfaces, stability can also be achieved.

IV. Derivation of the Admittance Boundary Condition

We present an example of transforming the acoustic liner admittance from the frequency-domain to the time-domain that is motivated by [14], in which a frequency-domain impedance boundary condition is translated to the time-domain using Fourier transforms.

Consider a geometric body with a surface that is treated with an acoustic liner. Assume a model with no mean flow; i.e., Mach number $M = 0$. Let $p(\boldsymbol{r}_s, \omega) = Z(\omega)v(\boldsymbol{r}_s, \omega)$ where $p(\boldsymbol{r}_s, \omega)$ is the acoustic pressure, $v(\boldsymbol{r}_s, \omega) = \boldsymbol{v} \cdot \boldsymbol{n}$, $\boldsymbol{v}$ is the acoustic velocity vector, $\boldsymbol{n}$ is the inward normal vector on the scattering body, and $Z(\omega)$ is the surface impedance. Then,

$$v(\boldsymbol{r}_s, \omega) = Y(\omega)p(\boldsymbol{r}_s, \omega), \tag{22}$$

where $Y(\omega) = 1/Z(\omega)$ is the surface admittance [14]. In the frequency-domain, v can be represented [9] by:

$$v(\boldsymbol{r}_s, \omega) = \frac{1}{i\omega\rho_0}\frac{\partial p}{\partial n}(\boldsymbol{r}_s, \omega), \tag{23}$$

where $\partial p/\partial n = P_n$ is the normal derivative of acoustic pressure defined by Eq. 12, ρ_0 is the average fluid density, and i is the imaginary unit ($i^2 = -1$).

Setting Eq. (22) equal to Eq. (23), we obtain a relation for $\partial p/\partial n$ in time-domain:

$$\frac{\partial p}{\partial n}(\boldsymbol{r}_s, t) = \frac{\rho_0}{2\pi}\int_{-\infty}^{t}\frac{\partial y}{\partial t}(t-\tau)p(\boldsymbol{r}_s, \tau)d\tau. \tag{24}$$

This results from using the inverse Fourier transform convolution property and causality condition which states: $y(t-\tau) = 0$ for all $t - \tau > 0$, i.e. $y(t-\tau) = 0$ for all $t > \tau$.

In [14], an *Extended Helmholtz Resonator Model* is proposed. In this model, the surface impedance is defined to be:

$$Z(\omega) = F_R + i\omega m - iF_\beta \cot\left(\frac{1}{2}\omega\nu\Delta t - i\frac{1}{2}\epsilon\right), \tag{25}$$

where for an acoustic liner represented by a wall consisting of an array of Helmholtz resonators:

F_R is the face-sheet resistance

ωm is the face-sheet mass reactance

$-\cot\left(\frac{1}{2}\omega\nu\Delta t - i\frac{1}{2}\epsilon\right)$ is the cavity reactance

F_β is a parameter used for varying the cavity reactance

Δt is the time-step

ϵ is the damping in the cavity's fluid, and

$\nu\Delta t = 2L/c$ is a multiple of the time-step and proportional to two times the cavity depth L divided by the speed of sound c

In (25), $F_R, m, L, c, \epsilon \geq 0$. The model is both passive [14]:

$$\mathrm{Re}(Z) = F_R + F_\beta\frac{\sinh(\epsilon)}{\cosh(\epsilon) - \cos(\omega\nu\Delta t)} > 0$$

and casual [14]:

$$\omega = \frac{2n\pi + i\epsilon}{\nu\Delta t},\ n \in \mathbb{Z}.$$

For $\mathrm{Im}(\omega) < \dfrac{\epsilon}{\nu\Delta t}$, (25) becomes:

$$Z(\omega) = F_R + i\omega m + F_\beta + 2F_\beta\sum_{N=1}^{\infty} e^{-i\omega N\nu\Delta t - \epsilon N} \tag{26}$$

which, by taking the inverse Fourier transform, leads to a time-domain representation of surface impedance:

$$z(t) = 2\pi \left[F_R \delta(t) + m\delta'(t) + F_\beta \delta(t) + 2F_\beta \sum_{N=1}^{\infty} e^{-\epsilon N} \delta(t - N\nu\Delta t) \right]. \tag{27}$$

In this work, we let the surface impedance be represented in the form of $Z(\omega) = A + iB$ where:

$$A = F_R + F_\beta \frac{\sinh(\epsilon)}{\cosh(\epsilon) - \cos(\omega_0 \nu \Delta t)} \text{ and } B = \omega_0 m - F_\beta \frac{\sin(\omega_0 \nu \Delta t)}{\cosh(\epsilon) - \cos(\omega_0 \nu \Delta t)} \tag{28}$$

are given at a specified frequency $\omega = \omega_0 > 0$ [14]. We assume a similar form for surface admittance, and obtain $Y(\omega) = \overline{A} + i\overline{B}$ such that:

$$\overline{A} = \frac{A}{A^2 + B^2} \text{ and } \overline{B} = \frac{-B}{A^2 + B^2}. \tag{29}$$

Matching the coefficients $\overline{A}$ and $\overline{B}$ using experimental data in [14], we obtain numerical values for $\overline{F_R}$ and $\overline{F_\beta}$ and may assume similar forms of Eqs. (26) and (27) for $Y(\omega)$ and $y(t)$, respectively. That is,

$$Y(\omega) = \overline{F_R} + i\omega m + \overline{F_\beta} + 2\overline{F_\beta} \sum_{N=1}^{\infty} e^{-i\omega N\nu\Delta t - \epsilon N}, \text{ and}$$

$$y(t) = 2\pi \left[\overline{F_R} \delta(t) + m\delta'(t) + \overline{F_\beta} \delta(t) + 2\overline{F_\beta} \sum_{N=1}^{\infty} e^{-\epsilon N} \delta(t - N\nu\Delta t) \right]. \tag{30}$$

Substituting (30) into (24), we obtain the derivation of an admittance boundary condition for soft surfaces:

$$\frac{\partial p}{\partial n}(\boldsymbol{r}_s, t) = \rho_0 \left(\overline{F_R} + \overline{F_\beta} \right) p'(\boldsymbol{r}_s, t) - \rho_0 m p''(\boldsymbol{r}_s, t) + 2\rho_0 \overline{F_\beta} \sum_{N=1}^{\infty} e^{-\epsilon N} p'(\boldsymbol{r}_s, t - N\nu\Delta t). \tag{31}$$

V. Coupling of the Admittance Boundary Condition

Consider the discretization of (31) at time t'. Let the solution for $p(\boldsymbol{r}_s, t)$ on S be expanded as in Eq. (17), and let the solution for $P_n(\boldsymbol{r}_s, t)$ on S_l be expanded as in Eq. (18). Substituting (12), (17), and (18) into (31), we get:

$$\begin{aligned} \sum_{k=0}^{N_t} \sum_{j=1}^{N_e} v_j^k \phi_j(\boldsymbol{r}_s) \psi_k(t') = \rho_0 \left(\overline{F_R} + \overline{F_\beta} \right) \sum_{k=0}^{N_t} \sum_{j=1}^{N_e} u_j^k \phi_j(\boldsymbol{r}_s) \psi_k'(t') - \rho_0 m \sum_{k=0}^{N_t} \sum_{j=1}^{N_e} u_j^k \phi_j(\boldsymbol{r}_s) \psi_k''(t') \\ + 2\rho_0 \overline{F_\beta} \sum_{k=0}^{N_t} \sum_{j=1}^{N_e} u_j^k \phi_j(\boldsymbol{r}_s) \left[\sum_{N=1}^{\infty} e^{-\epsilon N} \psi_k'(t' - N\nu\Delta t) \right]. \end{aligned} \tag{32}$$

Let the spatial and temporal basis functions be defined by Eqs. (19) and (20). By evaluating (32) at collocation points $\boldsymbol{r}_s = \boldsymbol{r}_i$ and time-step $t' = t_n$, we have:

$$\sum_{k=0}^{N_t} \sum_{j=1}^{N_e} v_j^k \delta_{ij} \psi_k(t_n) = \rho_0 \sum_{k=0}^{N_t} \sum_{j=1}^{N_e} u_j^k \delta_{ij} \left[\left(\overline{F_R} + \overline{F_\beta} \right) \psi_k'(t_n) - m\psi_k''(t_n) + 2\overline{F_\beta} \sum_{N=1}^{\infty} e^{-\epsilon N} \psi_k'(t_n - N\nu\Delta t) \right]. \tag{33}$$

The system of discretized equations (33) can be cast into the following matrix form with a finite number of K time steps:

$$\boldsymbol{D_0 u^n} + \boldsymbol{E_0 v^n} = -\boldsymbol{D_1 u^{n-1}} - \boldsymbol{E_1 v^{n-1}} - \boldsymbol{D_2 u^{n-2}} - \boldsymbol{E_2 v^{n-2}} - \ldots - \boldsymbol{D_K u^{n-K}} - \boldsymbol{E_K v^{n-K}} \tag{34}$$

where u^k and v^k denote the vector that contains all unknowns $\left\{ u_j^k,\ j = 1, ..., N_e \right\}$ and $\left\{ v_j^k,\ j = 1, ..., N_e \right\}$, respectively, at time level t_k. The non-zero entries for $\boldsymbol{D}$ and $\boldsymbol{E}$ are, respectively:

$$\{\boldsymbol{D_k}\}_{ij} = \delta_{ij} \rho_0 \left[\left(\overline{F_R} + \overline{F_\beta} \right) \psi_k'(t_n) - m\psi_k''(t_n) + 2\overline{F_\beta} \sum_{N=1}^{\infty} e^{-\epsilon N} \psi_k'(t_n - N\nu\Delta t) \right] \text{ and } \{\boldsymbol{E_k}\}_{ij} = \delta_{ij} \psi_k(t_n).$$

Equation (34) is a second system of equations for $\boldsymbol{u}^k$ and $\boldsymbol{v}^k$, which can be coupled with Eq. (21). Equations (21) and (34) form a March-On-in-Time scheme for the time-domain solution of the stable Burton-Miller type reformulation of Eq. (10). The coupled system can be expressed as:

$$\begin{bmatrix} \boldsymbol{B_0} & \boldsymbol{C_0} \\ \boldsymbol{D_0} & \boldsymbol{E_0} \end{bmatrix} \begin{bmatrix} \boldsymbol{u^n} \\ \boldsymbol{v^n} \end{bmatrix} = \begin{bmatrix} \boldsymbol{q^n} \\ \boldsymbol{0} \end{bmatrix} - \begin{bmatrix} \boldsymbol{B_1} & \boldsymbol{C_1} \\ \boldsymbol{D_1} & \boldsymbol{E_1} \end{bmatrix} \begin{bmatrix} \boldsymbol{u^{n-1}} \\ \boldsymbol{v^{n-1}} \end{bmatrix} - \cdots - \begin{bmatrix} \boldsymbol{B_K} & \boldsymbol{C_K} \\ \boldsymbol{D_K} & \boldsymbol{E_K} \end{bmatrix} \begin{bmatrix} \boldsymbol{u^{n-K}} \\ \boldsymbol{v^{n-K}} \end{bmatrix} - \cdots - \begin{bmatrix} \boldsymbol{B_J} & \boldsymbol{0} \\ \boldsymbol{0} & \boldsymbol{0} \end{bmatrix} \begin{bmatrix} \boldsymbol{u^{n-J}} \\ \boldsymbol{v^{n-J}} \end{bmatrix} \tag{35}$$

For locally reacting liners, the admittance boundary condition is given pointwise. It follows that the coefficients in Eq. (35) are all diagonal matrices. In fact, if the liner impedance is the same on all soft boundaries, we have coefficient matrices in the following form: $\boldsymbol{D_k} = d_k \boldsymbol{I}$ and $\boldsymbol{E_k} = e_k \boldsymbol{I}$ where $k = 0, 1, ..., K$, $\boldsymbol{I}$ is the identity matrix, and d_k, e_k are the coefficients for the time-domain liner admittance boundary condition that is the same for all liner elements.

VI. Eigenvalue Analysis

Due to the limited temporal stencil width shown in Eqs. (19) and (20), the $\boldsymbol{B}$ and $\boldsymbol{C}$ matrices in Eq. (21) and $\boldsymbol{D}$ and $\boldsymbol{E}$ matrices in Eq. (34) are sparse. The matrices $\boldsymbol{B_0}$, $\boldsymbol{C_0}$, $\boldsymbol{D_0}$, and $\boldsymbol{E_0}$ represent interactions within the same element or nearby nodes at the same time level t_n. Moreover, the matrices are diagonally dominant. In particular, the matrix $\boldsymbol{D}$ in Eq. (34) is a diagonal matrix whose coefficients simplify to:

$$d_k = \rho_0 \left(\overline{F_R} + \overline{F_\beta} \right) \begin{Bmatrix} 11/6, & k = 0 \\ -3, & k = 1 \\ 3/2, & k = 2 \\ -1/3, & k = 3 \\ 0, & \text{otherwise} \end{Bmatrix} - \rho_0 m \begin{Bmatrix} 2, & k = 0 \\ -5, & k = 1 \\ 4, & k = 2 \\ -1, & k = 3 \\ 0, & \text{otherwise} \end{Bmatrix} + 2\rho_0 \overline{F_\beta} \sum_{N=1}^{\infty} e^{-\epsilon N} \begin{Bmatrix} 11/6, & k - N\nu = 0 \\ -3, & k - N\nu = 1 \\ 3/2, & k - N\nu = 2 \\ -1/3, & k - N\nu = 3 \\ 0, & \text{otherwise} \end{Bmatrix}$$

and the matrix $\boldsymbol{E}$ in Eq. (34) is a diagonal matrix whose coefficients simplify to:

$$e_k = \begin{Bmatrix} 1, & k = 0 \\ 0, & k \neq 0 \end{Bmatrix}.$$

As mentioned in previous sections, direct numerical solution of the TD-BIE without the Burton-Miller type reformulation is prone to numerical instabilities. To study the stability of the coupled system given in Eq. (35), including the Burton-Miller type reformulation, we conduct a numerical eigenvalue study of the discretized system of equations [18].

Let us denote Eq. (35) by:

$$\boldsymbol{A_0 w^n} = \boldsymbol{q_0^n} - \boldsymbol{A_1 w^{n-1}} - \boldsymbol{A_2 w^{n-2}} - ... - \boldsymbol{A_J w^{n-J}} \tag{36}$$

such that

$$\boldsymbol{A_k} = \begin{bmatrix} \boldsymbol{B_k} & \boldsymbol{C_k} \\ \boldsymbol{D_k} & \boldsymbol{E_k} \end{bmatrix} \text{ for } k = 0, ..., K \text{ and } \boldsymbol{A_k} = \begin{bmatrix} \boldsymbol{B_k} & \boldsymbol{0} \\ \boldsymbol{0} & \boldsymbol{0} \end{bmatrix} \text{ for } k = K+1, ..., J, \ \boldsymbol{w^n} = \begin{bmatrix} \boldsymbol{u^n} \\ \boldsymbol{v^n} \end{bmatrix}, \text{ and } \boldsymbol{q_0^n} = \begin{bmatrix} \boldsymbol{q^n} \\ \boldsymbol{0} \end{bmatrix}.$$

We look for solutions of the form

$$\boldsymbol{w^n} = \lambda^n \boldsymbol{e_0} \tag{37}$$

to the corresponding homogeneous system given by Eq. (36). By substituting (37) into (36), we obtain a polynomial eigenvalue problem

$$\left[\boldsymbol{A_0} \lambda^J + \boldsymbol{A_1} \lambda^{J-1} + \boldsymbol{A_2} \lambda^{J-2} + \cdots + \boldsymbol{A_{J-1}} \lambda + \boldsymbol{A_J} \right] \boldsymbol{e_0} = 0$$

which can be cast into a generalized eigenvalue problem as follows:

$$\begin{bmatrix} -\boldsymbol{A_1} & -\boldsymbol{A_2} & \cdots & \cdots & -\boldsymbol{A_{J-1}} & -\boldsymbol{A_J} \\ \boldsymbol{I} & 0 & \cdots & \cdots & 0 & 0 \\ 0 & \boldsymbol{I} & \cdots & \cdots & 0 & 0 \\ \cdots & \cdots & \cdots & \cdots & \cdots & \cdots \\ 0 & 0 & \cdots & \cdots & 0 & 0 \\ 0 & 0 & \cdots & \cdots & \boldsymbol{I} & 0 \end{bmatrix} \begin{bmatrix} \boldsymbol{e_{J-1}} \\ \boldsymbol{e_{J-2}} \\ \cdot \\ \cdot \\ \boldsymbol{e_1} \\ \boldsymbol{e_0} \end{bmatrix} = \lambda \begin{bmatrix} \boldsymbol{A_0} & 0 & 0 & \cdots & 0 & 0 \\ 0 & \boldsymbol{I} & 0 & \cdots & 0 & 0 \\ 0 & 0 & \boldsymbol{I} & \cdots & 0 & 0 \\ \cdots & \cdots & \cdots & \cdots & \cdots & \cdots \\ 0 & 0 & 0 & \cdots & \boldsymbol{I} & 0 \\ 0 & 0 & 0 & \cdots & 0 & \boldsymbol{I} \end{bmatrix} \begin{bmatrix} \boldsymbol{e_{J-1}} \\ \boldsymbol{e_{J-2}} \\ \cdot \\ \cdot \\ \boldsymbol{e_1} \\ \boldsymbol{e_0} \end{bmatrix} \tag{38}$$

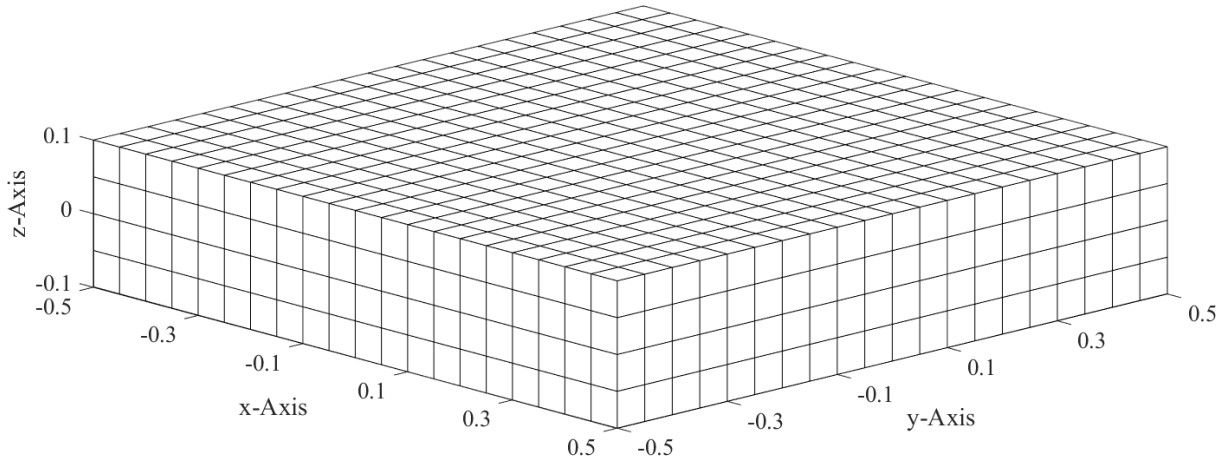

Fig. 2 Schematic diagram illustrating the $20 \times 20 \times 4$ surface discretization of the flat plate with dimension $[-0.5, 0.5] \times [-0.5, 0.5] \times [-0.1, 0.1]$, creating 1120 surface elements.

where $\boldsymbol{e_j} = \lambda^j \boldsymbol{e_0}$.

The numerical scheme given by either (35) or (36) is stable if $|\lambda| \leq 1$ for all eigenvalues of (38). Eigenvalues of the generalized eigenvalue problem (38) can be found via a sparse eigenvalue solver available in MATLAB or Python, or by a matrix power iteration method detailed in Appendix A.

For the stability study, we consider the scattering of an acoustic point source by a flat plate. The flat plate has dimension $[-0.5, 0.5] \times [-0.5, 0.5] \times [-0.1, 0.1]$ and the point source is located at $(x, y, z) = (0, 0, 1)$; the surface of the plate in the x-, y-, and z-directions is discretized using N_x, N_y, and N_z elements respectively. The time-domain admittance boundary condition (31) for this surface was developed using data from [14]. In [14], eighteen *Extended Helmholtz Resonator Models* are proposed for different frequency-domain combinations of $\mathrm{Re}(Z)$, $\mathrm{Im}(Z)$, and ν. These impedance models were converted into admittance conditions by taking values for $\mathrm{Re}(Z)$, $\mathrm{Im}(Z)$ and calculating values for $\mathrm{Re}(Y)$, $\mathrm{Im}(Y)$ using Eqs. (28) and (29). The coefficients $\overline{F_R}$ and $\overline{F_\beta}$ were then calculated and used to form the time-domain admittance boundary condition (31) and system of equations (35).

Several cases were assessed in the stability study by considering different combinations of $\mathrm{Re}(Z)$, $\mathrm{Im}(Z)$, ν, time-step, and problem size. We considered both positive and negative values for $\mathrm{Im}(Z)$, large and small ν, as well as two different time-steps and three different problem sizes including: $10 \times 10 \times 2$ (70 surface elements), $20 \times 20 \times 4$ (1120 surface elements), and $30 \times 30 \times 6$ (2520 surface elements). The $20 \times 20 \times 4$ discretization is illustrated in Figure 2. The values of the maximum eigenvalue for both the uncoupled system (21) — *rigid body only* — and coupled system (35) — *lined body* — are listed in Table 1. For the uncoupled cases, all eigenvalues are no greater than unity and stability is observed; these results were expected due to the Burton-Miller type reformulation of the TD-BEM. Moreover for the coupled cases, all eigenvalues are also no greater than unity and stability is once more observed. Stable results for the lined body coupled system were expected because acoustic liners are designed to impede sound. It is logical, therefore, that the addition of an admittance boundary condition would further stabilize an already-stable system.

VII. Concluding Remarks

A formulation of the acoustic wave scattering of geometric bodies treated with acoustic liners has been proposed. The current work uses an admittance boundary condition. The admittance boundary condition is derived and coupled with a TD-BIE which is stabilized with a Burton-Miller type reformulation to eliminate resonant frequencies in the interior domain. An iterative scheme is presented for the solution of the coupled system in time-domain which uses spatial and temporal basis functions and allows for acoustic scattering problems to be modeled with geometries consisting of both rigid and soft surfaces. Eigenvalue analysis was presented for both the uncoupled and coupled system. The uncoupled system — *rigid body only* — demonstrated stable solutions as to be expected due to the Burton-Miller type reformulation of the TD-BEM. The coupled system — *lined body* — also demonstrated stable solutions, in some cases with a slightly smaller maximum eigenvalue. It shows that, for the current formulation, the addition of an admittance

Table 1 Maximum eigenvalue, $|\lambda|_{\max}$, computed by Eq. (38) for the scattering by a flat plate with dimension $[-0.5, 0.5] \times [-0.5, 0.5] \times [-0.1, 0.1]$, for both uncoupled (rigid body) and coupled (rigid and lined body) cases, assessed for different combinations of Re(Z), Im(Z), ν, time-step, and problem size.

Time Step	$1/24$			$\pi/1000$	
$Z(\omega)$ from [14], $Y(\omega)$ *calculated*	$1 - 3i,\ 0.1 + 0.3i$			$1 - 3i,\ 0.1 + 0.3i$	
ν and ϵ, from [14]	$1,\ 0.0925419$			$1,\ 0.0925419$	
$\overline{F_R}$ and $\overline{F_\beta}$, *calculated*	$0.0674734,\ 0.5346532$			$0.1899699,\ -0.0516754$	
$N_x \times N_y \times N_z$	$10 \times 10 \times 2$	$20 \times 20 \times 4$	$30 \times 30 \times 6$	$20 \times 20 \times 4$	$30 \times 30 \times 6$
$\lvert\lambda\rvert_{\max}$, Uncoupled	**1.0000000**	**1.0000000**	**1.0000000**	**1.0000000**	**1.0000000**
$\lvert\lambda\rvert_{\max}$, Coupled	**0.9999038**	**0.9999732**	**0.9999814**	**1.0000000**	**1.0000000**
Time Step	$1/24$			$\pi/1000$	
$Z(\omega)$ from [14], $Y(\omega)$ *calculated*	$1 - 2i,\ 0.2 + 0.4i$			$1 - 2i,\ 0.2 + 0.4i$	
ν and ϵ, from [14]	$1,\ 0.1385102$			$1,\ 0.1385102$	
$\overline{F_R}$ and $\overline{F_\beta}$, *calculated*	$0.1349737,\ 0.7153618$			$0.3798652,\ -0.0757905$	
$N_x \times N_y \times N_z$	$10 \times 10 \times 2$	$20 \times 20 \times 4$	$30 \times 30 \times 6$	$20 \times 20 \times 4$	$30 \times 30 \times 6$
$\lvert\lambda\rvert_{\max}$, Uncoupled	**1.0000000**	**1.0000000**	**1.0000000**	**1.0000000**	**1.0000000**
$\lvert\lambda\rvert_{\max}$, Coupled	**0.9999745**	**0.9999932**	**0.9999953**	**1.0000000**	**1.0000000**
Time Step	$1/24$			$\pi/1000$	
$Z(\omega)$ from [14], $Y(\omega)$ *calculated*	$1 - i,\ 0.5 + 0.5i$			$1 - i,\ 0.5 + 0.5i$	
ν and ϵ, from [14]	$1,\ 0.2738691$			$1,\ 0.2738691$	
$\overline{F_R}$ and $\overline{F_\beta}$, *calculated*	$0.3377861,\ 0.9106569$			$0.9486897,\ -0.1402522$	
$N_x \times N_y \times N_z$	$10 \times 10 \times 2$	$20 \times 20 \times 4$	$30 \times 30 \times 6$	$20 \times 20 \times 4$	$30 \times 30 \times 6$
$\lvert\lambda\rvert_{\max}$, Uncoupled	**1.0000000**	**1.0000000**	**1.0000000**	**1.0000000**	**1.0000000**
$\lvert\lambda\rvert_{\max}$, Coupled	**0.9999997**	**1.0000000**	**1.0000000**	**1.0000000**	**1.0000000**
Time Step	$1/24$			$\pi/1000$	
$Z(\omega)$ from [14], $Y(\omega)$ *calculated*	$1 + i,\ 0.5 - 0.5i$			$1 + i,\ 0.5 - 0.5i$	
ν and ϵ, from [14]	$19,\ 0.2738691$			$19,\ 0.2738691$	
$\overline{F_R}$ and $\overline{F_\beta}$, *calculated*	$0.7363680,\ -1.5748604$			$0.9486897,\ -0.1402522$	
$N_x \times N_y \times N_z$	$10 \times 10 \times 2$	$20 \times 20 \times 4$	$30 \times 30 \times 6$	$20 \times 20 \times 4$	$30 \times 30 \times 6$
$\lvert\lambda\rvert_{\max}$, Uncoupled	**1.0000000**	**1.0000000**	**1.0000000**	**1.0000000**	**1.0000000**
$\lvert\lambda\rvert_{\max}$, Coupled	**1.0000000**	**1.0000000**	**1.0000000**	**1.0000000**	**1.0000000**
Time Step	$1/24$			$\pi/1000$	
$Z(\omega)$ from [14], $Y(\omega)$ *calculated*	$1 + 2i,\ 0.2 - 0.4i$			$1 + 2i,\ 0.2 - 0.4i$	
ν and ϵ, from [14]	$19,\ 0.1385102$			$19,\ 0.1385102$	
$\overline{F_R}$ and $\overline{F_\beta}$, *calculated*	$0.2947523,\ -1.2407070$			$0.3798652,\ -0.0757905$	
$N_x \times N_y \times N_z$	$10 \times 10 \times 2$	$20 \times 20 \times 4$	$30 \times 30 \times 6$	$20 \times 20 \times 4$	$30 \times 30 \times 6$
$\lvert\lambda\rvert_{\max}$, Uncoupled	**1.0000000**	**1.0000000**	**1.0000000**	**1.0000000**	**1.0000000**
$\lvert\lambda\rvert_{\max}$, Coupled	**1.0000000**	**1.0000000**	**1.0000000**	**1.0000000**	**1.0000000**
Time Step	$1/24$			$\pi/1000$	
$Z(\omega)$ from [14], $Y(\omega)$ *calculated*	$1 + 3i,\ 0.1 - 0.3i$			$1 + 3i,\ 0.1 - 0.3i$	
ν and ϵ, from [14]	$19,\ 0.0925419$			$19,\ 0.0925419$	
$\overline{F_R}$ and $\overline{F_\beta}$, *calculated*	$0.1473958,\ -0.9278081$			$0.1899699,\ -0.0516754$	
$N_x \times N_y \times N_z$	$10 \times 10 \times 2$	$20 \times 20 \times 4$	$30 \times 30 \times 6$	$20 \times 20 \times 4$	$30 \times 30 \times 6$
$\lvert\lambda\rvert_{\max}$, Uncoupled	**1.0000000**	**1.0000000**	**1.0000000**	**1.0000000**	**1.0000000**
$\lvert\lambda\rvert_{\max}$, Coupled	**1.0000000**	**1.0000000**	**1.0000000**	**1.0000000**	**1.0000000**

boundary condition would further stabilize an already-stable system.Future work will include solving for the acoustic pressure on soft surfaces and comparing scattering solutions to those obtained for rigid bodies and studying different acoustic liner models to assess scattering at a broader band of frequencies.

Acknowledgments

F. Q. Hu and M. E. Pizzo are supported by a NASA Cooperative Agreement, NNX11AI63A. M. E. Pizzo is also supported in part by an Old Dominion University Modeling and Simulation graduate fellowship. This work used the computational resources at the Old Dominion University ITS Turing cluster and the Extreme Science and Engineering Discovery Environment (XSEDE), which is supported by National Science Foundation grant number OCI-1053575.

Appendix A

We describe a matrix power iteration method for finding the largest eigenvalue of (38). Let

$$\boldsymbol{A} = \begin{bmatrix} -\boldsymbol{A_0}^{-1}\boldsymbol{A_1} & -\boldsymbol{A_0}^{-1}\boldsymbol{A_2} & \cdots & \cdots & -\boldsymbol{A_0}^{-1}\boldsymbol{A_{J-1}} & -\boldsymbol{A_0}^{-1}\boldsymbol{A_J} \\ \boldsymbol{I} & 0 & \cdots & \cdots & 0 & 0 \\ 0 & \boldsymbol{I} & \cdots & \cdots & 0 & 0 \\ \cdots & \cdots & \cdots & \cdots & \cdots & \cdots \\ 0 & 0 & \cdots & \cdots & 0 & 0 \\ 0 & 0 & \cdots & \cdots & \boldsymbol{I} & 0 \end{bmatrix}. \tag{39}$$

Then, the power iteration method proceeds as follows [19]. Given an arbitrary unit vector $\boldsymbol{e^{(0)}}$, and for $k = 1, 2, ...,$ compute:

$$\boldsymbol{w}^{(k)} = \boldsymbol{A}\boldsymbol{e^{(k-1)}},\ \boldsymbol{e^{(k)}} = \frac{\boldsymbol{w}^{(k)}}{||\boldsymbol{w}^{(k)}||_2},\ \text{and eigenvalue } \lambda^{(k)} = \left[\boldsymbol{e^{(k)}}\right]^T \boldsymbol{A}\boldsymbol{e^{(k)}} = \left[\boldsymbol{e^{(k)}}\right]^T \boldsymbol{w}^{(k+1)}.$$

The iteration is stopped when $|\lambda^{(k)} - \lambda^{(k-1)}|/|\lambda^{(k)}| < \epsilon$, where ϵ is the tolerance and set to be 10^{-12}. When the iteration is convergent, it converges to the largest eigenvalue of $\boldsymbol{A}$, i.e., $|\lambda|_{\max}$.

References

[1] Hu, F. Q., "An Efficient Solution of Time Domain Boundary Integral Equations for Acoustic Scattering and Its Acceleration by Graphics Processing Units," *19th AIAA/CEAS Aeroacoustics Conference*, Vol. 2013-2018, American Institute of Aeronautics and Astronautics, Washington, DC, 2013.

[2] Hu, F. Q., "Further Development of a Time Domain Boundary Integral Equation Method for Aeroacoustic Scattering Computations," *20th AIAA/CEAS Aeroacoustics Conference*, Vol. 2014-3194, American Institute of Aeronautics and Astronautics, Washington, DC, 2014.

[3] Hu, F. Q., Pizzo, M. E., and Nark, D. M., "On the Assessment of Acoustic Scattering and Shielding by Time Domain Boundary Integral Equation Solutions," *22nd AIAA/CEAS Aeroacoustics Conference*, Vol. 2016-2779, American Institute of Aeronautics and Astronautics, Washington, DC, 2016.

[4] Hu, F. Q., Pizzo, M. E., and Nark, D. M., "A New Formulation of Time Domain Boundary Integral Equation for Acoustic Wave Scattering in the Presence of a Uniform Mean Flow," *23rd AIAA/CEAS Aeroacoustics Conference*, Vol. 2017-3510, American Institute of Aeronautics and Astronautics, Washington, DC, 2017.

[5] Chappell, D. J., Harris, P. J., Henwood, D., and Chakrabarti, R., "A Stable Boundary Element Method for Modeling Transient Acoustic Radiation," *Journal of the Acoustical Society of America*, Vol. 120, No. 1, 2006, pp. 74–80.

[6] Ergin, A. A., Shankar, B., and Michielssen, E., "Analysis of Transient Wave Scattering from Rigid Bodies Using a Burton-Miller Approach," *Journal of the Acoustical Society of America*, Vol. 106, No. 5, 1999, pp. 2396–2404.

[7] Jones, A. D., and Hu, F. Q., "A Three-Dimensional Time-Domain Boundary Element Method for the Computation of Exact Green's Functions in Acoustic Analogy," *13th AIAA/CEAS Aeroacoustics Conference*, Vol. 2007-3479, American Institute of Aeronautics and Astronautics, Washington, DC, 2007.

[8] Marburg, S., "The Burton and Miller Method: Unlocking Another Mystery of Its Coupling Parameter," *Journal of Computational Acoustics*, Vol. 23, No. 1550016, 2015.

[9] Marburg, S., and Schneider, S., "Influence of Element Types on Numeric Error for Acoustic Boundary Elements," *Journal of Computational Acoustics*, Vol. 11, No. 3, 2001, pp. 363–386.

[10] Astley, R. J., and Macaulay, G. J., "Three-Dimensional Wave-Envelope Elements of Variable Order for Acoustic Radiation and Scattering. Part I. Formulation in the Frequency Domain," *Journal of the Acoustical Society of America*, Vol. 103, No. 1, 1998, pp. 49–63.

[11] Kierkegaard, A., Boij, S., and Efraimsson, G., "A Frequency Domain Linearized Navier-Stokes Equations Approach to Acoustic Propogation in Flow Ducts with Sharp Edges," *Journal of the Acoustical Society of America*, Vol. 142, No. 4, 2010, pp. 710–719.

[12] Iob, A., Arina, R., and Schipani, C., "Frequency-Domain Linearized Euler Model for Turbomachinery Noise Radiation Through Engine Exhaust," *American Institute of Aeronautics and Astronautics Journal*, Vol. 48, No. 4, 2010, pp. 848–858.

[13] Tam, C. K. W., and Auriault, L., "Time-Domain Impedance Boundary Conditions for Computational Aeroacoustics," *American Institute of Aeronautics and Astronautics Journal*, Vol. 34, No. 5, 1996, pp. 917–923.

[14] Rienstra, S. W., "Impedance Models in Time Domain Including the Extended Helmholtz Resonator Model," *12th AIAA/CEAS Aeroacoustics Conference*, Vol. 2006-2686, American Institute of Aeronautics and Astronautics, Washington, DC, 2006.

[15] Spillere, A. M. N., Medeiros, A. A., and Cordiolo, J. S., "An Improved Impedance Education Technique Based on Impedance Models and the Mode Matching Method," *Applied Acoustics*, Vol. 129, No. 2018, 2017, pp. 322–334.

[16] Morse, P. M. ., and Ingard, K. U., *Theoretical Acoustics*, 1st ed., Princeton University Press, Princeton, 1986.

[17] Hu, F. Q., Pizzo, M. E., and Nark, D. M., "On a Time Domain Boundary Integral Equation Formulation for Acoustic Scattering by Rigid Bodies in Uniform Mean Flow," *Journal of the Acoustical Society of America*, Vol. 142, No. 6, 2017, pp. 3624–3636.

[18] Dodson, S. J., Walker, S. P., and Bluck, M. J., "Impicitness and Stability of Time Domain Integral Equation Scattering Analysis," *Applied Computational Electromagnetics Society Journal*, Vol. 13, 1998, pp. 291—301.

[19] Golub, G. H., and Loan, C. F. V., *Matrix Computation*, 4th ed., Johns Hopkins University Press, Baltimore, 2013.